Received: 9 October 2021 | Revised: 27 May 2022 | Accepted: 29 May 2022

DOI: 10.1002/met.2080

RESEARCH ARTICLE

Meteorological Applications
Science and Technology for Weather and Climate
Open Access
RMetS

Performance evaluation of a high-resolution regional model over West Africa for operational use: A case study of August 2017

Eniola A. Olaniyan[1] | **Carlo Cafaro**[2] | **Stephen B. Ogungbenro**[3] | **Imoleayo E. Gbode**[3] | **Vincent O. Ajayi**[3] | **Ayodeji Oluleye**[3] | **Elijah A. Adefisan**[3] | **Juliane Schwendike**[4] | **Kamoru A. Lawal**[1,5]

[1]Deparment Weather Forecasting Services Numerical Weather Prediction, Nigerian Meteorological Agency (NiMet), Abuja, Nigeria

[2]Department of Meteorology, University of Reading, Reading, UK

[3]School of Earth and Mineral Science Department of Meteorology and Climate Science, Federal University of Technology, Akure, Nigeria

[4]Department of Meteorology, School of Earth and Environment, University of Leeds, Leeds, UK

[5]African Climate and Development Initiative, University of Cape Town, Cape Town, South Africa

Correspondence
Eniola A. Olaniyan, Nigerian Meteorological Agency (NiMet), Abuja, Nigeria.
Email: olaniyan.eniola67@gmail.com

Funding information
Global Challenges Research Fund, Grant GCRF African SWIFT, Grant/Award Number: NE/P021077/1

Abstract

The frequency of flash floods resulting from heavy rainfall over West Africa has increased in recent years with serious socio-economic consequences. Therefore, the need to utilize numerical weather prediction models to forecast heavy rainfall events reliably is also rising at many operational meteorological centres in West Africa. This paper evaluates the performance of the Consortium for Small-scale Modelling (COSMO) model of the German Meteorological Services (DWD) in predicting rainfall over West Africa for high-impact rainfall events that occurred between 19 and 26 August 2017. The paper aims to investigate the synoptic forcings modulating daily rainfall variability during that period. Results show that COSMO simulates adequately the spatio-temporal variability of rainfall distribution over West Africa, though with inherent biases. COSMO displays a decreasing skill in producing spatial rainfall distribution as rainfall amounts tend to 30 mm and above. Additionally, areas of heavy rainfall, mostly about 100–300 km southwest of the core of the Africa Easterly Jet (AEJ), often coincide with areas of decreasing mean sea level pressure of at least 0.6 hPa and areas of increasing convective available potential energy of at least 500 J/kg. Although not in all cases, the trough of the Africa Easterly Wave (AEW) is always located to the east of these areas. We show that not every storm, especially east of the prime meridian, is associated with an AEW trough. COSMO is able to reproduce the atmospheric dynamics modulating the daily rainfall variability, in addition to capturing the daily propagation of the AEW trough, and the core of the AEJ. However, the reproducibility skill of the model in predicting atmospheric dynamics may not transform into the predictive skill of the model in producing rainfall. Nevertheless, operational forecasters may be able to determine likely areas of heavy rainfall by estimating the position of the AEJ core based on the position of areas of the least falling pressure from COSMO. Finally, the incorporation of the fractions skill

This is an open access article under the terms of the Creative Commons Attribution-NonCommercial License, which permits use, distribution and reproduction in any medium, provided the original work is properly cited and is not used for commercial purposes.
© 2022 The Authors. *Meteorological Applications* published by John Wiley & Sons Ltd on behalf of Royal Meteorological Society.

score metric based on the neighbourhood approach could also assist operational forecasters to decide at which scale a severe weather alert can be issued.

KEYWORDS
African SWIFT, COSMO model, evaluation, FSS, heavy rainfall, West Africa

1 | INTRODUCTION

Rainfall is the most important atmospheric component in operational weather forecasting over West Africa, and the most difficult one to predict. This is because rainfall affects not only everyday life, but also agriculture, hydrology, civil defence, and a variety of other human and socio-economic activities (Rakesh & Goswami, 2016). As a result, reliable rainfall forecasting is critical in most decision-making for socio-economic sustainability, in agriculture, for example, rainfall forecasts can be utilized in crop selection, sowing schedules, irrigation, and pesticide application (e.g., Sivakumar, 2006).

West African rainfall, either on daily, decadal, monthly, or seasonal timescale, is driven, intensified, and sustained by consistent interactions between various global drivers (Giannini et al., 2003; Hoerling et al., 2006; Olaniyan et al., 2019; Zeng et al., 1999).

Some of these drivers, in this study and particularly for operational practice, include the mean sea level pressure (MSLP; Lavaysse et al., 2009); the African Easterly Jet (AEJ; Afiesimama, 2007; Wu et al., 2010); Africa Easterly Waves (AEWs; Diedhiou et al., 1999); and the convective available potential energy (CAPE; Chen et al., 2020; Gartzke et al., 2017; Olaniyan et al., 2015; Ziarani et al., 2019). For instance, studies have shown that the teleconnection between both the AEJ and AEW is yet to be fully understood (Asnani, 2005; Cook, 1999; Grogan et al., 2017). According to these studies, the AEW derives its energy through the barotropic–baroclinic instability from the AEJ. Consequently, the consensus is that the AEJ has the strongest impact on the occurrence of rainfall in West Africa. On the other hand, CAPE and MSLP are widely used by West African National Meteorological and Hydrological Services (WA-NMHS) to quantify atmospheric instability that aids convection. Studies have found a positive correlation between CAPE and rainfall accumulation (e.g., Chen et al., 2020). With the increased trust in and the utilization of climate models by WA-NMHS, it is vital that models adequately represent and capture monsoon complexes and the modulating mechanisms over the region. This paper aims to examine how well the Consortium for Small-scale Modelling (COSMO) can reproduce these modulating mechanisms. This analysis will establish the validity of using COSMO over West Africa, especially for high-impact weather such as heavy rainfall.

1.1 | Predictive skill of COSMO

The predictive skills of COSMO over the years have been investigated in different regions of the world for different purposes. In Germany Hauck et al. (2011) analysed the discrepancies between observed and modelled soil moisture fields and their potential impacts on convective precipitation forecasts. To achieve this, operational and high-resolution simulations with the weather forecast system GME/COSMO-DE were merged with soil moisture monitoring data from the Convective and Orographically-induced Precipitation Study 2007. They found that soil moisture has a considerable impact on convection-related parameters over complex and heterogeneous terrain. Over Antarctica, Wacker et al. (2009) investigated a weather episode characterized by synoptic disturbances using COSMO. By comparing the model simulations with observation, they demonstrated that the model may show some inherited biases, but it captured well the general meteorological conditions including the timing and rainfall amounts. Similarly, over Germany, Akkermans et al. (2012) used a regime-dependent evaluation technique to assess the model performance of two COSMO variants (COSMO-DE and COSMO-EU), in distinguishing synoptic patterns. Using COSMO-EU, a 7-km grid spacing model, they identified a strong windward/leeward orographic effect. This way, they concluded that COSMO-EU strongly overestimates precipitation at windward sides and underestimates at crest and lee sides.

Notwithstanding the different studies identifying the performance of COSMO over different regions, few studies have focused on the performance of the 7-km COSMO over West Africa. This is despite the study of Olaniyan et al. (2015), which used COSMO at 7 km grid spacing to study the daily evolution of the West African Monsoon (WAM) over Nigeria for the first half of 2015. They concluded that the model can qualitatively predict the daily evolution of the WAM over Nigeria. The aforementioned shards of research still leave fundamental questions unanswered in using COSMO in operational weather forecasting. First, can a better understanding of the

teleconnection between synoptic processes and areas of heavy rainfall contribute to better COSMO forecast interpretation? Second, can the neighbourhood method improve the COSMO forecasts in detecting areas of heavy rainfall?

Some National Weather and Hydrological Centres in West Africa are collaborating with scientists globally as part of the African Science for Weather Information and Forecasting Techniques (African SWIFT) project (https://africanswift.org/). The project collaboration aims to develop sustainable African weather forecasting capability (Parker et al., 2021).

Although convection-permitting (CP) ensembles forecasts were produced as part of SWIFT to get users more acquainted with ensemble-based products during major testbeds in the project, due to economic challenges, adopting an operational CP ensemble forecast system may not be currently feasible in West Africa. Therefore, investigating the COSMO's predictive abilities over the region will be of great operational benefit in the long term, as COSMO is one of the operational numerical weather prediction models used at the Nigerian Meteorological Agency and other West African weather services. One of such operational benefits is the WMO Severe Weather Forecasting Services (SWFP) in West Africa.

1.2 | Operational evaluation metrics

To evaluate the skill of COSMO, we implemented the neighbourhood approach, a spatial verification method to generate and to verify rainfall forecasts to overcome the so-called 'double penalty' problem (Gilleland et al., 2009). Traditional verification scores (e.g., root mean square error or contingency table score), when applied to high-resolution forecasts and grid points, are inadequate because they could penalize twice for not predicting the event where it is observed (miss) and for predicting it where it has not been observed (false alarm).

Here the neighbourhood method has been applied to the COSMO deterministic model, for different neighbourhood sizes and rainfall thresholds. This method was introduced by Theis et al. (2005) to produce probabilistic forecasts from a deterministic model using an inexpensive approach. Fractions of grid points exceeding a fixed threshold or a percentile have been calculated from either forecasts or observations. The fractions skill score (FSS; Roberts & Lean, 2008) has then been used as a verification metric to compare these forecast fractions to assess the ability of the model to predict the location of rainfall. FSS is sensitive also to the model bias, so a percentiles threshold has been used to remove the effect of the bias and to focus solely on the quantification of the displacement error (Skok & Roberts, 2016).

Since its introduction, the FSS has become a widely used verification metric to monitor the performance of the different forecasting models, mainly for studies over extra-tropical regions. Arguably, one of the reasons it became a popular metric is because FSS can be used to determine the spatial scale at which a forecast is deemed to be 'useful'. Using this as a metric makes the FSS easier to interpret by the end-users. More precisely, the useful scale is defined as the smallest scale at which FSS ≥ 0.5 (Skok & Roberts, 2016). Recently, the FSS has been used for evaluating forecasting models in Tropical East Africa (Cafaro et al., 2021; Hanley et al., 2021; Woodhams et al., 2018). To the best of our knowledge, this study would be the first to apply the FSS metric in the West Africa domain from deterministic COSMO simulations.

1.3 | Current operational practice and evaluation

For operational weather forecasts, many meteorological centres, especially in developed countries, rely on numerical weather prediction (NWP) systems (Baldauf et al., 2011; Saito et al., 2006; Staniforth & Wood, 2008). Rainfall forecasts are simulated in most of these countries using a high-resolution CP ensemble prediction system, which has helped to increase the efficiency of high-impact weather (HIW) forecasting (Cuo et al., 2011).

Despite significant progress in the use of NWP in developed worlds, most countries, especially in West Africa, lack the resources needed to create a robust operational NWP system. This is despite few countries with limited capability to run parameterized deterministic limited-area models. COSMO for example is a high-resolution regional model used at the Nigerian Meteorological Agency (NiMet), which depends on the lateral boundary and initial conditions from the German Weather Services (DWD) for weather simulations (Majewski et al., 2002).

Fundamentally, quantitative precipitation forecasts with deterministic models according to various studies (Clark et al., 2009; Maurer et al., 2017) have some underlying disadvantages. For instance, because of inherent errors in modelling and observational systems, deterministic forecasts of atmospheric states even at a very high spatial resolution are difficult beyond 12-h lead time (Bongioannini et al., 2005; Clark et al., 2009; Cuo et al., 2011). Despite these shortcomings, many operational centres in West Africa, such as NiMet and the Ghana Meteorological Agency (GMet), still depend on high-resolution deterministic models to provide daily rainfall forecasts for decision-making. As a result, it is critical to establish a rigorous assessment methodology that is adapted to

best operational practices to reduce the inherent biases by using deterministic models. Therefore, this study will use a case study of storm events from 19 to 26 August 2017 to fill a research void over West Africa using COSMO.

1.4 | The rainfall events of 19–27 August 2017

Between 19 and 26 August 2017, a sequence of mesoscale convective systems (MCSs) passed over West Africa. Heavy rainfall was triggered by the propagating systems along their path, resulting in flooding in many areas across the region. One such event is the worst flood event since 2012 in Benue State in Nigeria, which was a result of the overflow of river Benue (https://reliefweb.int/report/niger/west-and-central-africa-2017-flood-impact-18-oct-2017/). The socio-economic consequences of this flooding event are enormous (https://www.vanguardngr.com/2017/09/benue-flood-gov-ortom-raises-alarm/). According to Nigeria's National Emergency Management Agency, over 100,000 people were displaced, and over 4000 homes were destroyed in the state's 12 local government areas. Other countries affected during these events are the Niger Republic, with an estimation of 200 thousand displaced people, Guinea with almost 3500 affected people and 10 deaths, and Ghana, which has an estimation of 3000 displaced people and recorded 7 deaths (https://reliefweb.int/report/niger/west-and-central-africa-2017-flood-impact-18-oct-2017). Furthermore, according to several studies (Fischer et al., 2020; Kimberlain et al., 2015; Kowaleski et al., 2020; Senkbeil et al., 2019), the intertwining systems culminated in Hurricane Irma (30 August–12 September 2017), the fifth most devastating hurricane in US history (https://www.weather.gov/mfl/hurricaneirma). This study, therefore, aims to evaluate the performance of COSMO in reproducing the heavy rainfall triggered by the MCSs that occurred between 19 and 27 August 2017.

2 | DATA AND METHODS

2.1 | COSMO set-up

This study is based on the COSMO model (Baldauf et al., 2011). It is configured to have a horizontal grid spacing of approximately 7 km with 50 vertical levels and a terrain-following coordinate system (Lorenz grid staggering). COSMO is a non-hydrostatic limited-area atmospheric prediction model that takes into account a variety of physical processes (Kober et al., 2015; Ritter & Geleyn, 1992). Among these is the radiative transfer scheme by Majewski et al. (2002), the deterministic Tiedtke parameterization of convection (Tiedtke, 1989), and the Mironow

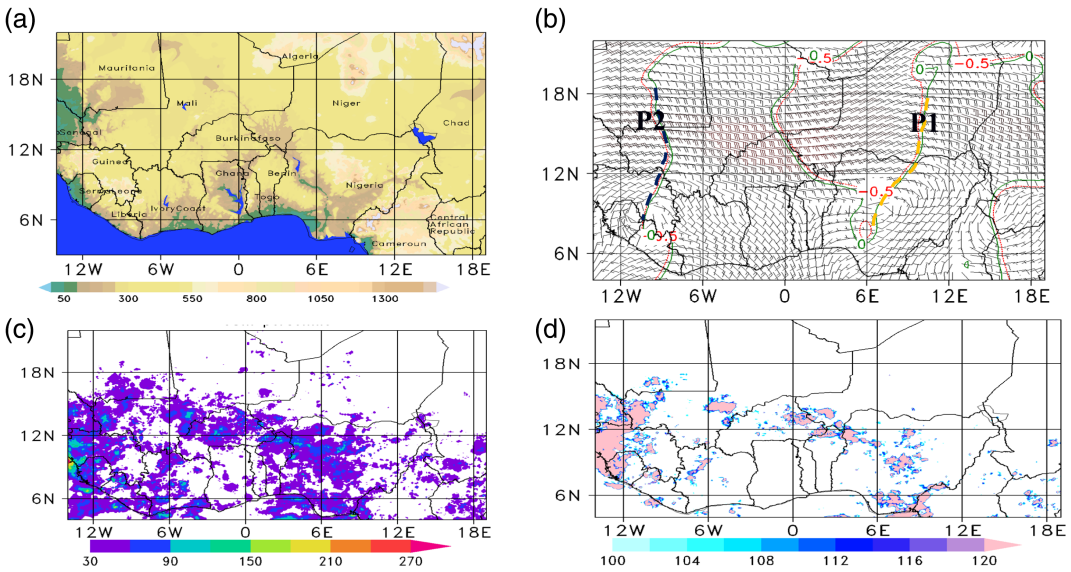

FIGURE 1 Maps showing (a) topography of the COSMO-model domain, (b) wind flow at 600 mb (wind barbs: Red barbs are the areas of jet streams), broken yellow and blue lines indicate the positions of the trough axes to the east (P1) and the west (P2) of the prime meridian, respectively, determined from the 0 meridional winds (green contour) and the 0.5-kn meridional wind (red contour) based on ERAI, (c) the 95th percentile of rainfall accumulation (mm), and (d) spatial distribution of rainfall accumulation (mm) from 19 to 26 August 2017 based on GPM-IMERG. COSMO, Consortium for Small-scale Modelling; GPM-IMERG, Integrated Multi-satellite Retrieval for Global Precipitation Measurement.

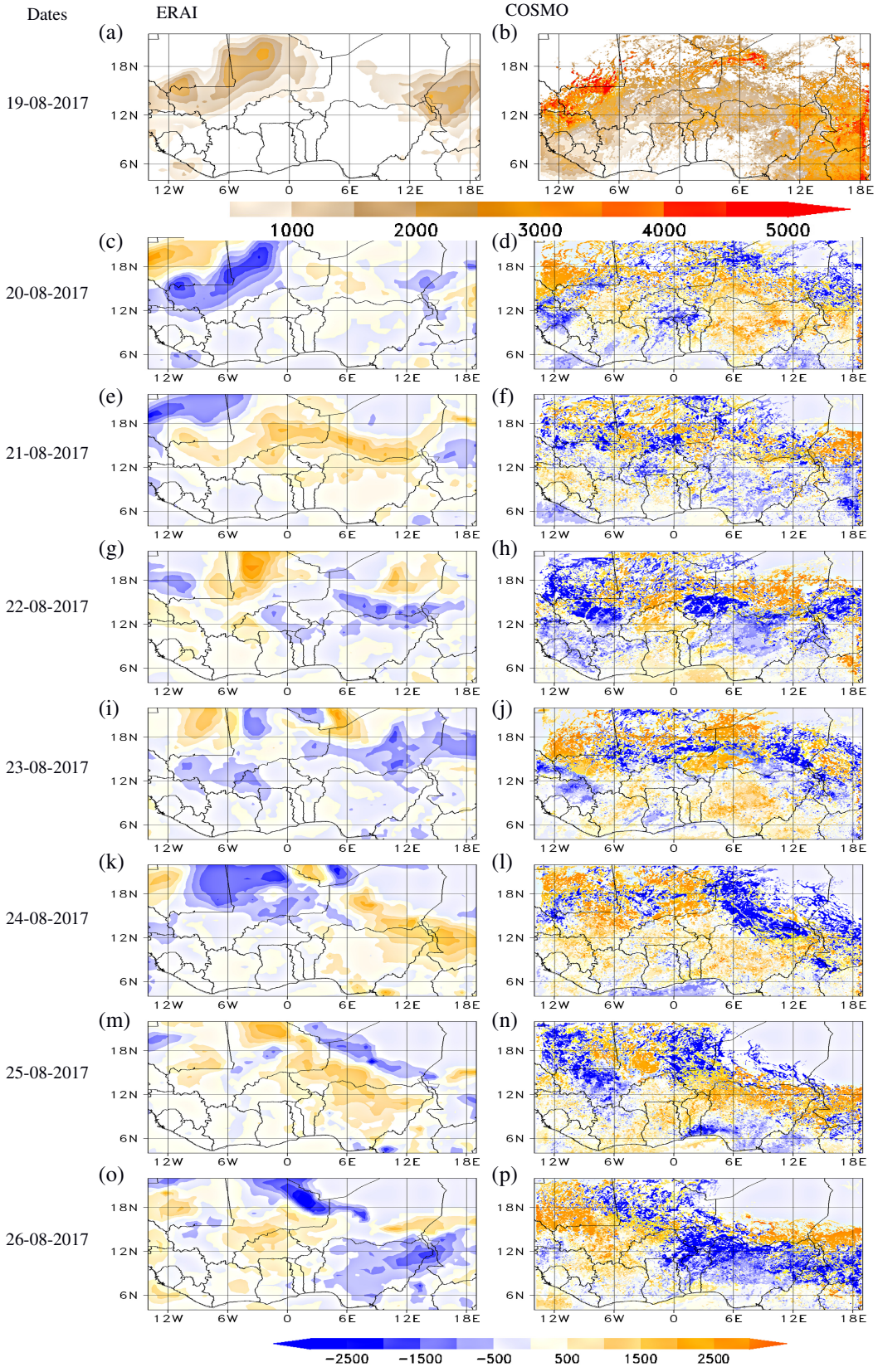

FIGURE 2 CAPE (a) based on ERAI on 19 August 2017, and (b) as simulated daily for 19 August 2017. CAPE tendencies based on ERAI (c,e,g,i,k,m,o), and as simulated daily (d,f,h,j,l,n,p) from 20 to 26th August 2017. CAPE, convective available potential energy.

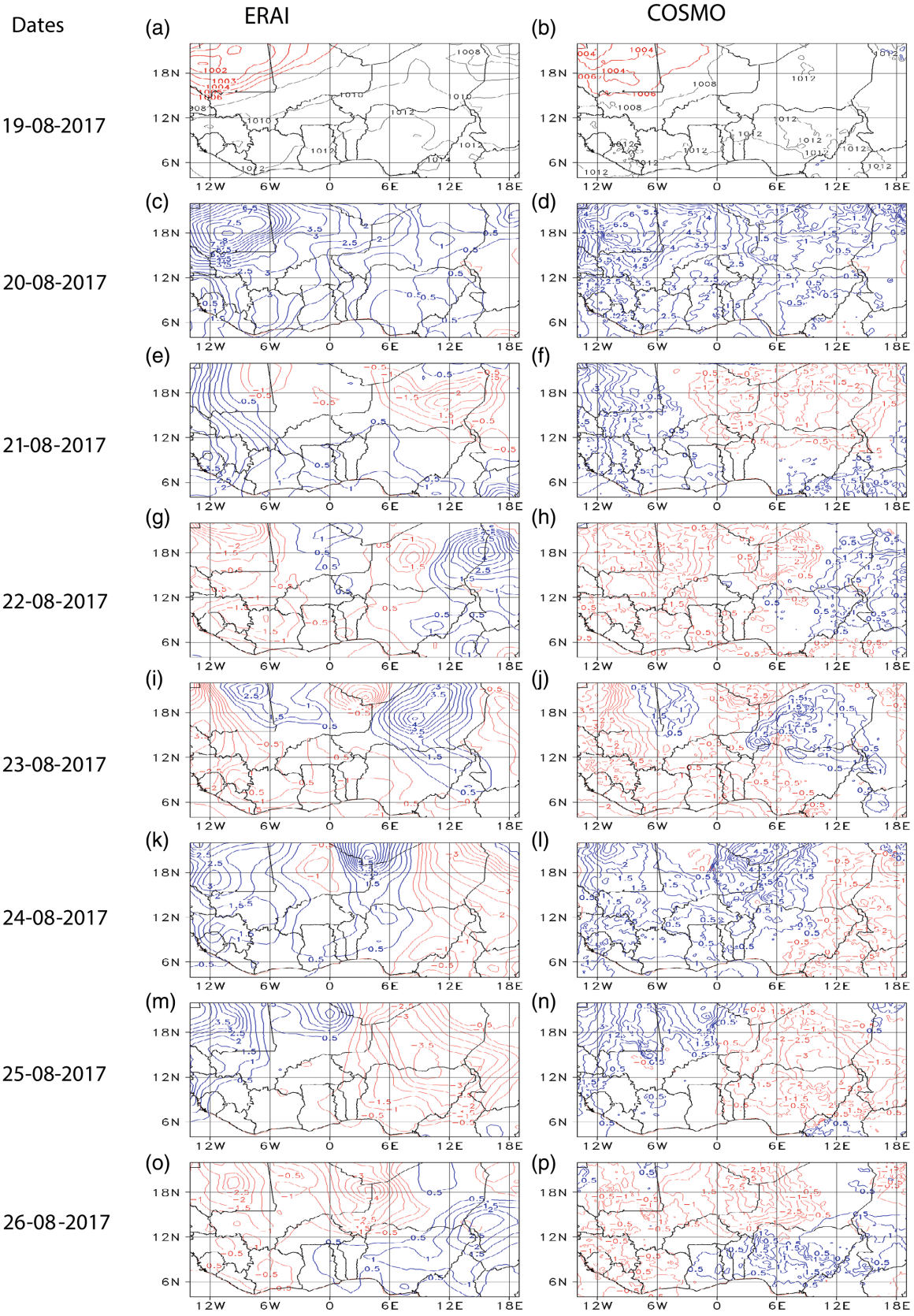

FIGURE 3 MSLP (a) based on ERAI on 19 August 2017 (the red contours indicate areas of low pressure and the blue contour indicating areas of high pressure), and (b) as simulated daily by COSMO. Pressure tendency based on ERAI (c,e,g,i,k,m,o) and (d,f,h,j,l,n,p) as simulated daily by COSMO (red contours indicate areas of falling pressure and the blue contours indicate areas of rising pressure) from 20–26th August 2017. COSMO, Consortium for Small-scale Modelling.

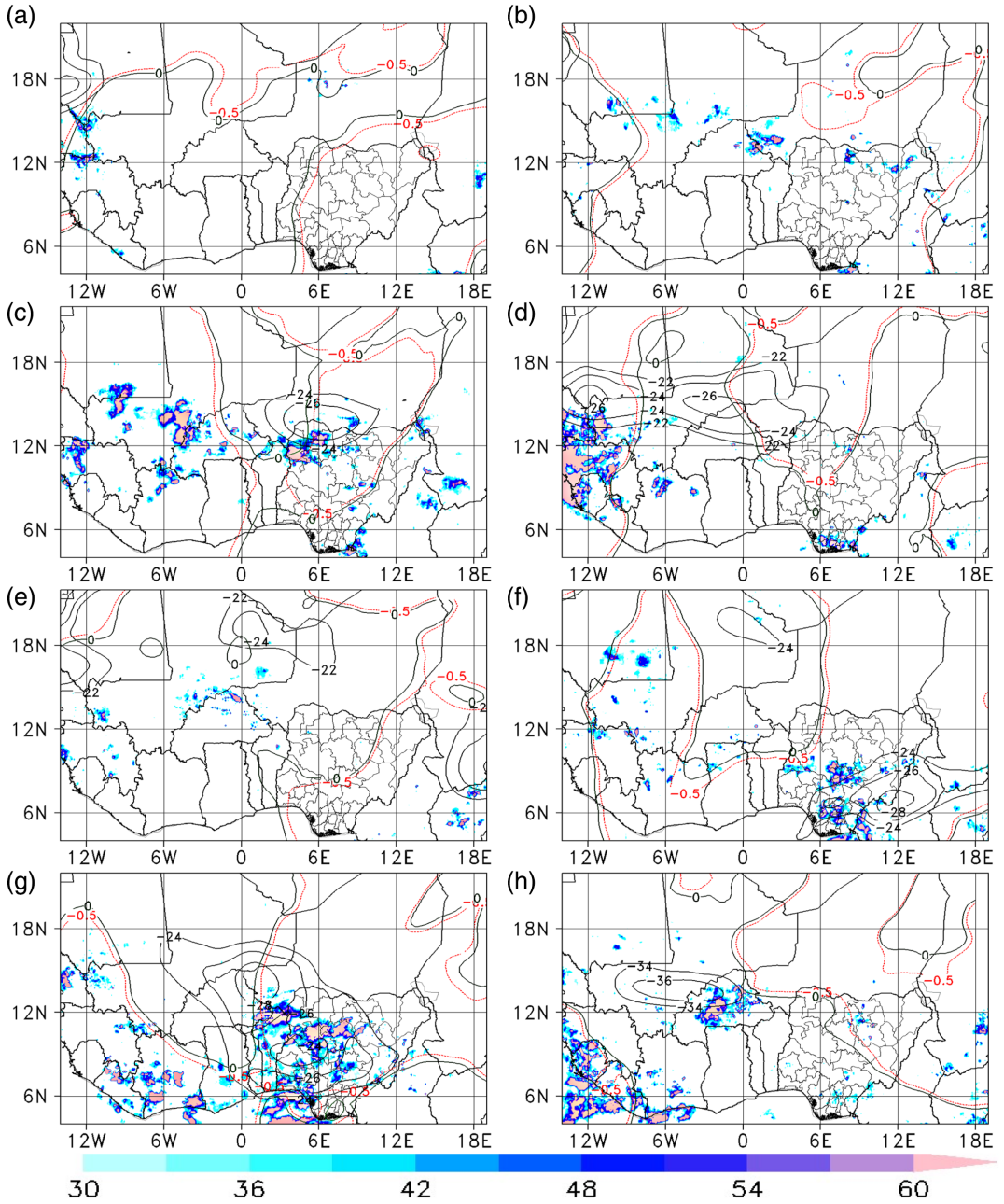

FIGURE 4 Spatial distribution of daily accumulated rainfall above 30 mm (shaded) based on GPM-IMERG, the AEJ (zonal wind [knots]; black contours) and AEW trough (meridional wind [knots]; coloured lines are 0.0 kn [dark green] and −0.5 kn [red]) at 600 mb from (a) the 19 to (h) 26 August 2017 based on ERAI. AEJ, Africa Easterly Jet; AEW, Africa Easterly Wave; GPM-IMERG, Integrated Multi-satellite Retrieval for Global Precipitation Measurement.

turbulence scheme (Mironov & Raschendorfer, 2001). The scheme is based on prognostic turbulent kinetic energy closure at level 2 according to Mellor and Yamada (1982) and the stochastic Plant–Craig convection parameterization (Groenemeijer & Craig, 2012; Kain & Michael, 1990). The microphysics scheme of COSMO includes riming processes (graupel formation) and is formulated as a Lin-type one-moment cloud microphysics scheme that predicts cloud water, rainwater, cloud ice, snow, and graupel (Lin et al., 1983).

The model is run on a regular gridded domain of −14° to 19°E longitude and 3° to 22°N latitude covering West African countries, as shown in Figure 1a. With a 7-km horizontal grid spacing, the model has 529 × 305 grid points. COSMO is forced by 3-hourly initial and boundary conditions derived from an interpolation analysis of the 13-km Icosyhedral Non-hydrostatic Global Model (ICON) run by the DWD (Ritter & Geleyn, 1992). The model is initialized at 0000UTC each day of the case study period for 60 h and output is provided at 3 h intervals.

2.2 | Precipitation and reanalysis data

Rainfall networks over Africa are sparse (Washington et al., 2006; Woodhams et al., 2018). Therefore, satellite-derived observed daily rainfall data from the Integrated Multi-satellite Retrieval for Global Precipitation Measurement (GPM-IMERG) (Skofronick-Jackson et al., 2017) is used in this study. GPM-IMERG data are available every 30 min at 10-km grid spacing and covers the whole globe. Although GPM has some inherent biases (Maranan et al., 2020; Stein et al., 2019), several studies (Cafaro et al., 2021; Stein et al., 2019; Woodhams et al., 2018) have used GPM for model verification, especially over Africa. Here, the GPM data are retrieved every 30 min from 19 to 27 August 2017.

European Centre for Medium Range Forecasts Reanalysis ERA-Interim (hereafter: ERAI) at 14 km grid spacing every 6 h was used (Dee et al., 2011). The ERAI reanalysis data are used to determine the teleconnections between the global driving forcings and the daily rainfall characteristic with an emphasis on heavy rainfall. Heavy rainfall is classified in this study as daily rainfall amounts greater than 30 mm. This threshold is in line with the NiMet operational practice. The minimum of the 95th percentile of the daily rainfall accumulation within the period of interest corresponds to approximately 30 mm (Figure 1c).

2.3 | Methods

From GPM-IMERG and COSMO, the 24-h daily rainfall accumulation is computed using the World Meteorological Organisation (WMO) operational standard. It implies that the daily rainfall accumulation of present day (PD) is the rainfall accumulation from 0600 UTC of the PD to 0600 UTC of the next day (ND). The sourced variables from the ERAI and the COSMO simulations are the zonal (u) and meridional (v) winds at 700, 650, and 600 hPa levels, respectively, which are used to investigate the AEJ and AEW. Also sourced are the MSLP and CAPE. The daily mean horizontal wind is computed between the 0600 of PD and 0600 of ND as the mean wind for the PD for ease of reference with the rainfall accumulation. The zonal wind is used to determine the spatio-temporal position of the AEJ. To determine the axis and the core of the AEJ (hereafter, AEJ pool), only areas with the highest zonal wind, plus 5 kn at 700, 650, and 600 hPa are analysed, which is different from other studies that are using predetermined threshold values of 10–12 ms^{-1} (20–25 kn) (Afiesimama, 2007; Cook, 1999). In this study, the AEW trough is used to identify the AEW. The AEW trough location is determined using the meridional wind, where

TABLE 1 Estimated average position of the AEW trough.

	700 mb				650 mb				600 mb			
Date	ERAI-P1	ERAI-P2	COSMO-P1	COSMO-P2	ERAI-P1	ERAI-P2	COSMO-P1	COSMO-P2	ERAI-P1	ERAI-P2	COSMO-P1	COSMO-P2
20	17°E	4°E	16°E	10°E	16.5°E	4°E	15°E	ud	16°E	>14°W	15°E	13
21	13°E	2°W	15°E	2°W	13°E	2	14°E	2	12°E	2	10.5°E	0
22	9°E	9°W	10°E	5°W	9°E	9	11°E	5	9°E	8	9°E	6
23	4°E	12°W	3°E	12°W	3°E	12	3°E	10	ud	10	3°E	13
24	17°E	4°W	17°E	12°W	17°E	4	16°E	2	17°E	4	17°E	2
25	13°E	8°W	12°E	7°W	13.5°E	10	ud	8	13°E	9	10°E	7
26	ud	11°W	ud	12°W		12	ud	12	12/ud	12	ud	12

Note: In ERA and as simulated daily by COSMO (P1 = position one of the wave troughs, P2 = position two of the wave trough and ud = undetermined position).
Abbreviations: AEW, Africa Easterly Wave; COSMO, Consortium for Small-scale Modelling.

the meridional wind at the level of the AEJ is equal to zero. Here, based on common operational practices, that location is defined as the wave trough where the wind shifts from northerlies to southerlies (Figure 1b). Then, the mean position of the wave trough is subjectively determined from the upper longitudinal and the lower longitudinal positions of the trough. The extent and interaction of daily atmospheric instability are diagnosed using the CAPE and MSLP. Here, we considered the highest daily CAPE value and derive its daily variability (tendency) by computing the deviation of the PD CAPE from that of the ND CAPE. The element of the MSLP considered in this study is the pressure tendency, which is the deviation of the PD MSLP from that of the ND MSLP to indicate if the surface pressure of the ND is rising or falling. Quantitative statistical metrics that address the spatio-temporal discrimination, reliability, and resolution of COSMO such as linear correlation and phase composite to determine the performance of COSMO in producing the global drivers in the ERAI reanalysis were utilized. For ease of comparison, COSMO output was re-gridded to the ERAI resolution (14 km).

The rainfall forecast from the COSMO is used to objectively evaluate the skill of the modelled daily evolution and rainfall distribution. For the evaluation, COSMO is re-gridded to 10-km grid spacing to be compared with GPM. We then compute the linear correlation and biases to assess model reliability. Additionally, this study uses FSS by utilizing the neighbourhood method for testing potential improvement in the model spatial skill in predicting heavy rainfall. The FSS is computed for selected areas on selected days using rainfall threshold exceeding 95th percentile, within an increasing neighbourhood of 30, 50, 70, 110, 150, 210, 270, and 310 km.

3 | RESULTS

3.1 | Rainfall teleconnection

The observed maximum daily CAPE on 19 August, as shown in Figure 2a, ranges from 1500 to 3000 J kg^{-1}. However, the daily variability of CAPE tendency differs over different areas with positive CAPE tendency, moving westwards (Figure 2c,e,g,i,k,m,o). On 21–22 August, for instance, the increased CAPE tendency, as shown in Figure 2e,g, which covers almost the entire area north of 10°N, shifts westward, covering areas such as Senegal, Guinea, Sierra Leone, and Liberia. Similarly, in Figure 2k,m,o, the CAPE tendency increases east of the prime meridian on 24 August and covers most of Nigeria on 25 August. The area of positive CAPE tendency moves westwards to cover areas of the west of the prime meridian. The CAPE tendency becomes less positive over

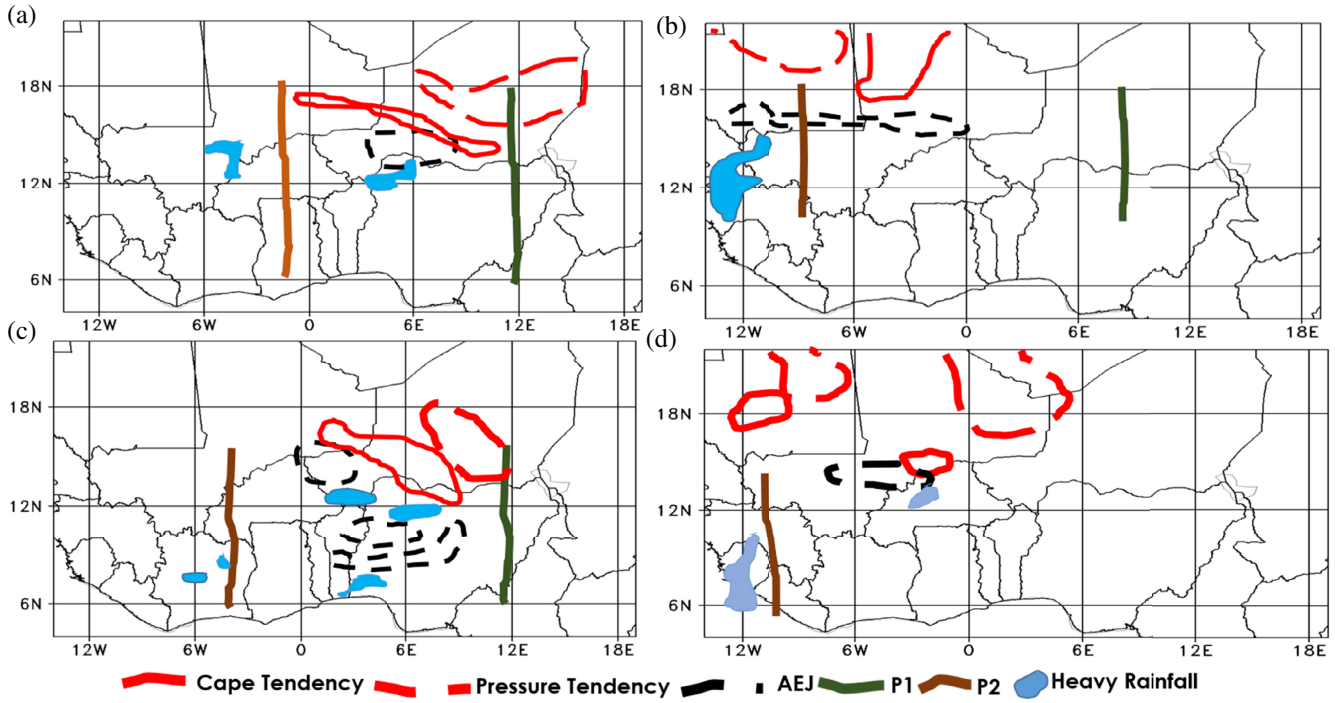

FIGURE 5 Synthetic analysis showing the interaction between modulating drivers (CAPE, MSLP, AEJ Core, AEW through positions 1 and 2 (P1 and P2), and areas of heavy daily rainfall distribution on (a) 21 August 2017, (b) 22 August 2017, (c) 25 August 2017, and (d) 26 August 2017. AEJ, Africa Easterly Jet; AEW, Africa Easterly Wave; CAPE, convective available potential energy; MSLP, mean sea level pressure.

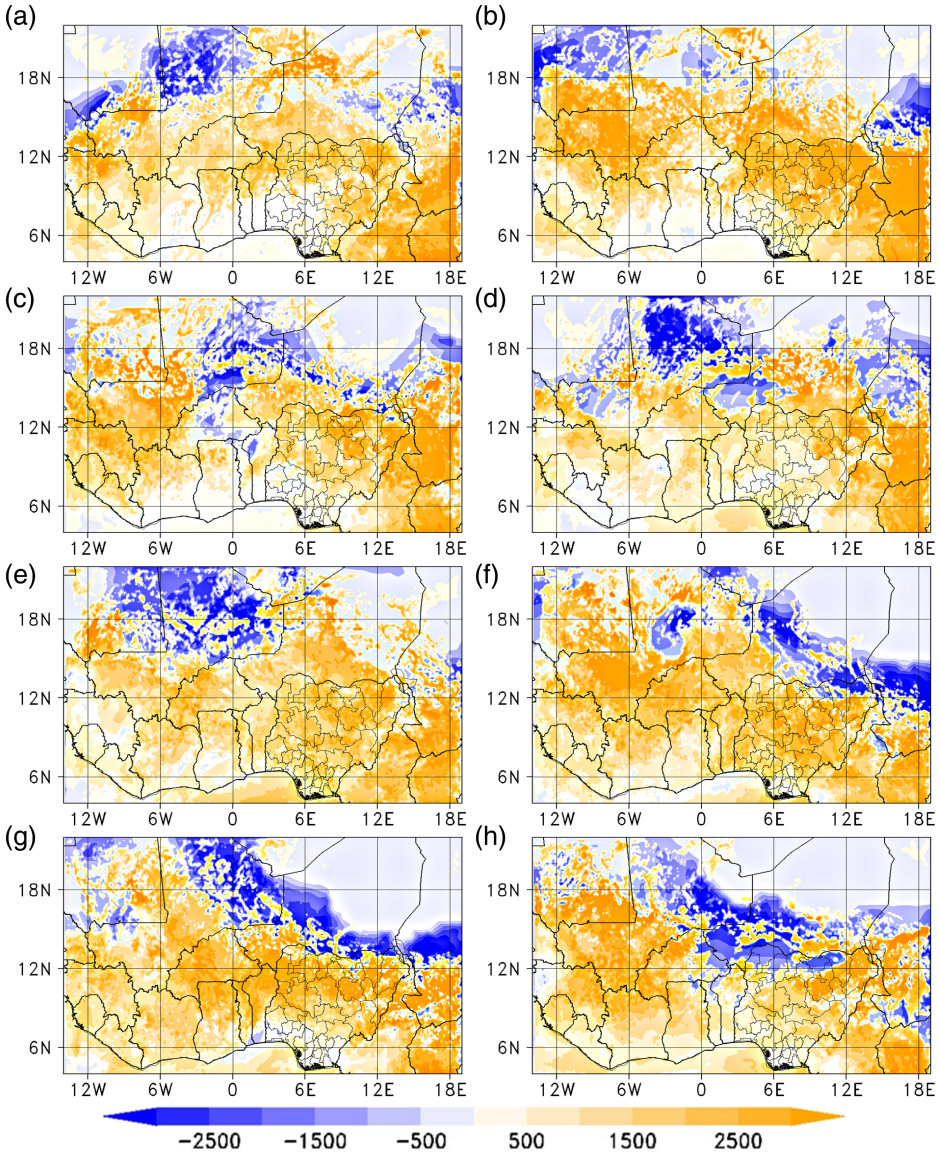

FIGURE 6 Map showing the COSMO bias of CAPE based on ERAI from (a) the 19th to (h) 26th August 2017. CAPE, convective available potential energy; COSMO, Consortium for Small-scale Modelling.

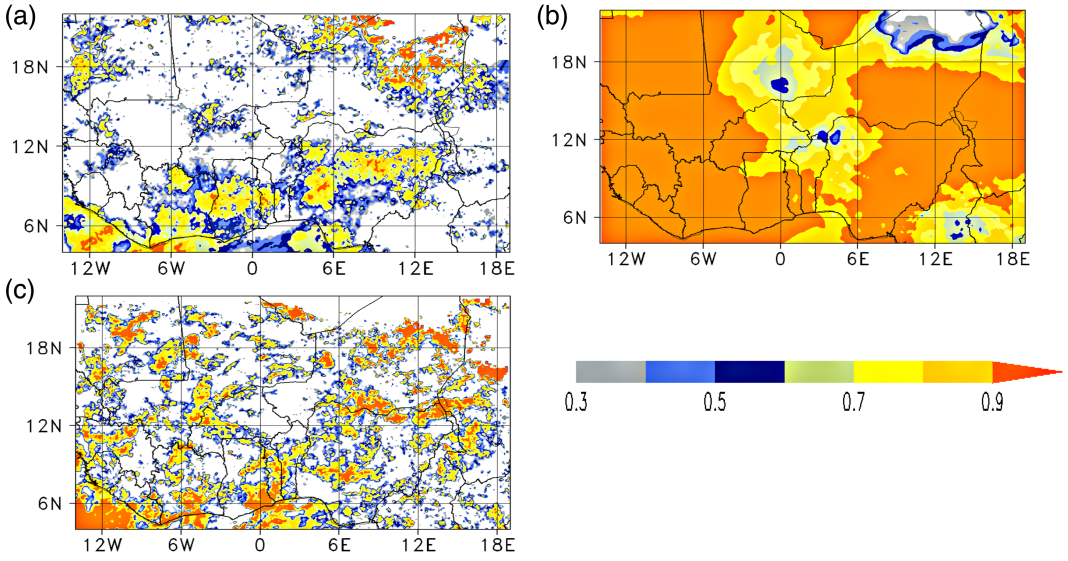

FIGURE 7 Map showing the correlation between COSMO and (a) ERAI CAPE, (b) ERAI MSLP, and (**c**) GPM-IMERG daily rainfall accumulation. CAPE, convective available potential energy; COSMO, Consortium for Small-scale Modelling; GPM-IMERG, Integrated Multi-satellite Retrieval for Global Precipitation Measurement.

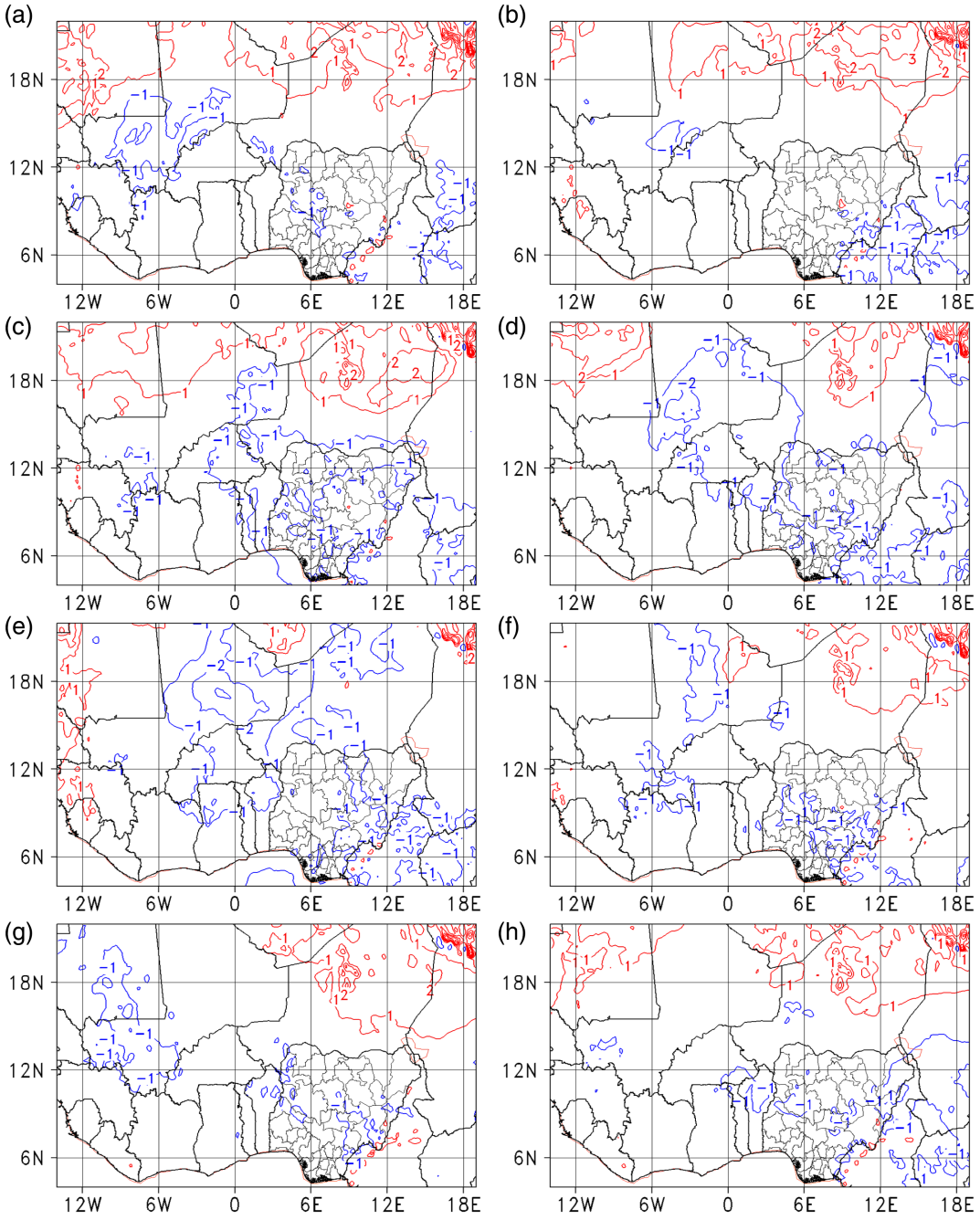

FIGURE 8 Map showing the MSLP bias between COSMO and ERAI from the (a) the 19th to (h) 26th August 2017 with the red lines indicating a positive bias and the blue lines a negative bias. COSMO, Consortium for Small-scale Modelling; MSLP, mean sea level pressure.

Nigeria on 26 August. The spatio-temporal characteristics of the surface pressure (Figure 3c,e,g,i,k,m,o) suggest that most areas of falling or rising pressure coincides with areas of increased or decreased CAPE tendency. The few areas of exception are over north-western Nigeria, north-eastern Benin, and southern Mali on 21 August (Figure 3e).

The position of the AEW trough at 600 hPa is shown in Figure 4 and is consistent with the position at 650 and 700 hPa. At all three levels, two wave troughs of varying speed move across West Africa from the east to the west. The first wave trough on 20 August is located at approximately 17°E. Although not observed at 600 hPa, the second wave trough located approximately 4°E at both 650 and 700 hPa (not shown) is shallower than the first trough. By 24 August (Figure 4f and Table 1), the first wave trough on 20 August has moved to about 4°E, and another wave trough was observed at approximately 17°E. On average, the trough (P1) moves westward with a daily speed of about 444 km day^{-1}.

The spatio-temporal characteristic of the AEJ (Figure 4) is consistent at 600, 650, and 700 hPa, except

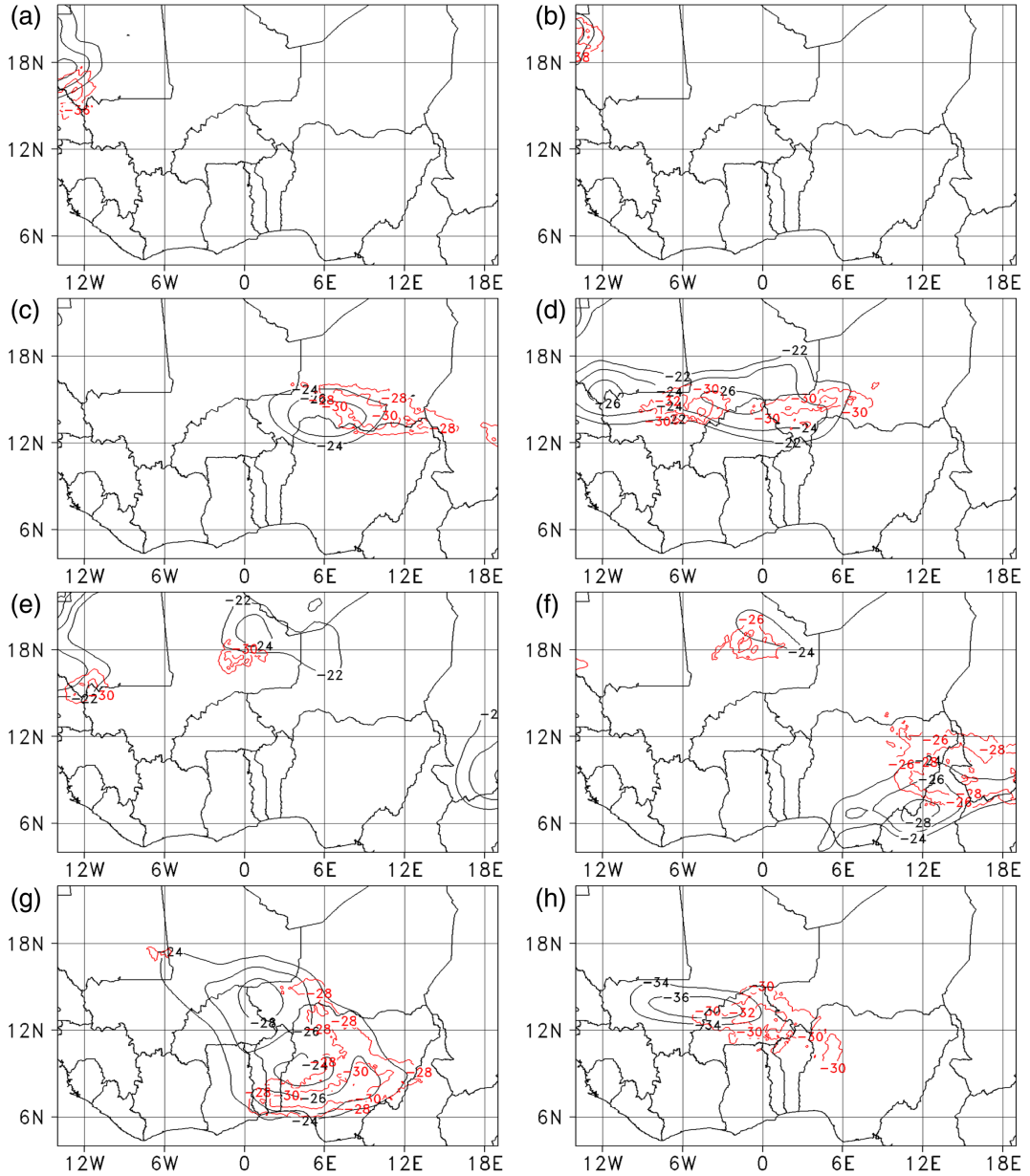

FIGURE 9 Spatial position of the AEJ core (zonal wind, knots) at 600 mb based on ERAI in black contour and as simulated daily by COSMO model in red contour from (a) 19 to (h) 26 August 2017. AEJ, Africa Easterly Jet; COSMO, Consortium for Small-scale Modelling.

on 24 August at the 700 hPa level (not shown). Figure 4 also shows the position of the AEJ core, which includes isolated wind speed maxim north of 16°N on 23 and 24 August (Figure 4e,f), respectively. Despite the similarities in strength and position of the AEJ core at 600, 650, and 700 hPa, there are also unique deviations. For instance, on 22 August (Figure 4d), the AEJ axis is linking two AEJ cores extending from Senegal to Burkina Faso at both 600 hPa and 650 hPa (not shown). On the contrary, the second AEJ core over Senegal is absent at 700 hPa (not shown). Likewise, the observed incursion of a deep pool of AEJ over northern Nigeria at 700 hPa (not shown) on 24 August is observed as a maximum at both 600 hPa (Figure 4f) and 650 hPa (not shown) on the same day. At all three levels, the observed AEJ pool generally as shown in (Figure 5) lies between two AEW troughs with the core of the jet sometimes overlapping with the areas of most increasing CAPE, to the south of the least falling pressure, shifting in concert with the westward movement of the troughs.

The interaction between the forcings resulted in accumulated rainfall of greater than 120 mm (Figure 1d) in many areas across West Africa between 19 and 27 August. As depicted in Figure 4, daily accumulated rainfall greater than 30 mm is observed over different regions each day but with similar attributes at all levels. Areas of

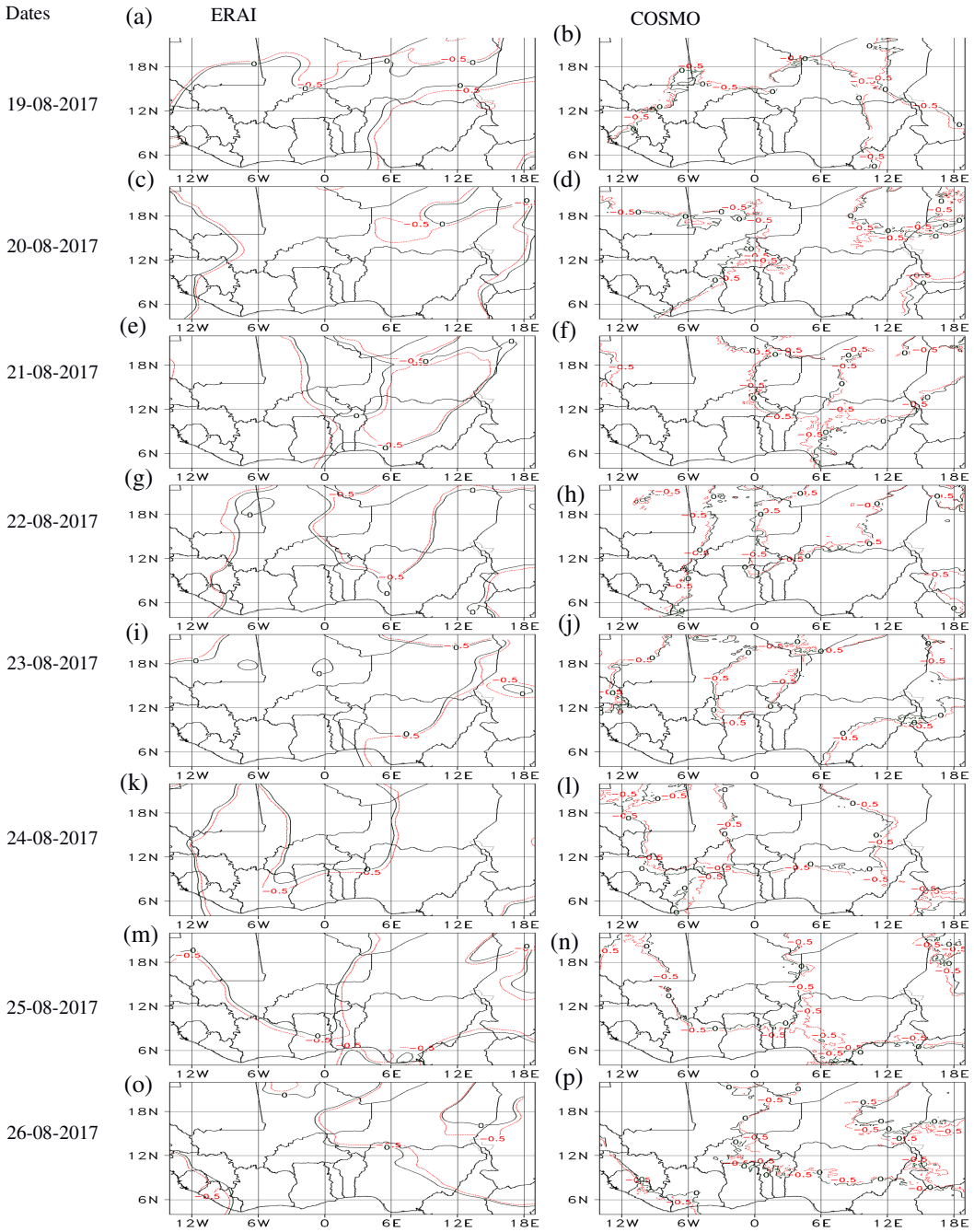

FIGURE 10 AEW based on ERAI (c,e,g,i,k,m,o), and (d,f,h,j,l,n,p) as simulated daily by COSMO from 19 to 26th August 2017. The coloured lines are 0.0 kn (0 m/s) (green) and −0.5 kn (−0.25 m/s) (red) and represent the AEW wave trough at 600 mb. AEW, Africa Easterly Wave; COSMO, Consortium for Small-scale Modelling.

rainfall greater than 30 mm lie and move ahead of the AEW trough; they are observed to occur within the AEJ pool but frequently south of the AEJ axis (Figure 4d), including the AEJ entrance (south-east; Figure 4h) and the AEJ exit (southwest; Figure 4c,f).

Furthermore, as depicted in Figures 2–4, areas of heavy rainfall may not always be connected with areas of falling pressure (Figures 3e and 4e), but they are frequently linked with increasing buoyancy (CAPE). Additionally, areas of widespread rainfall amount greater than 30 mm are areas where falling surface pressure and increasing CAPE tendency coincide.

3.2 | Synoptic forcings

The COSMO model simulations can reproduce the daily spatio-temporal characteristics and variability of CAPE

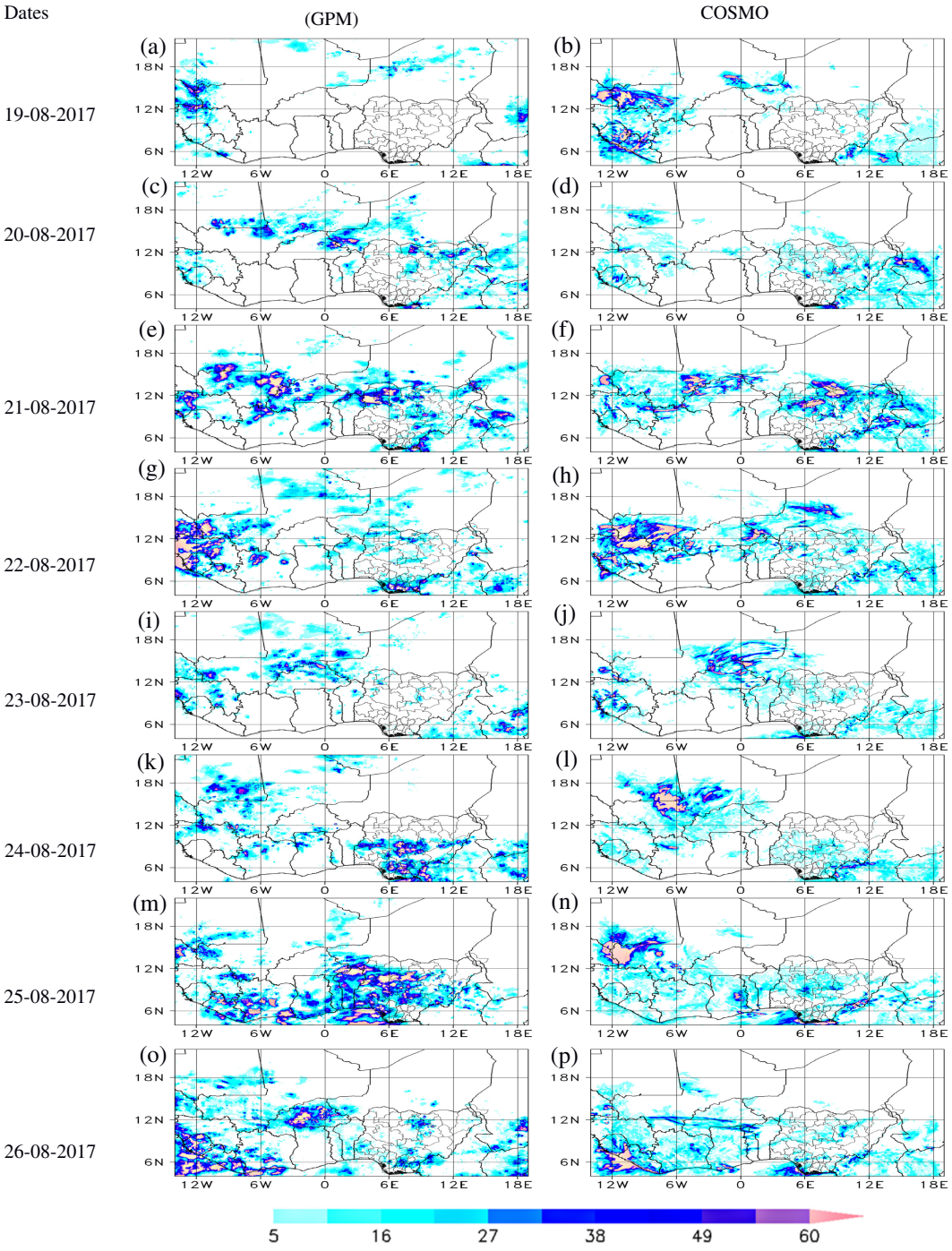

FIGURE 11 Spatial distribution of daily rainfall accumulation above 5 mm based on GPM-IMERG (c,e,g,i,k,m,o), and (d,f,h,j,l,n,p) as simulated daily by COSMO from 19 to 26th August 2017. COSMO, Consortium for Small-scale Modelling; GPM-IMERG, Integrated Multi-satellite Retrieval for Global Precipitation Measurement.

and MSLP, with underlying biases (Figures 6 and 7). For instance, the model generally overestimates the atmospheric buoyancy (CAPE) over many areas south of latitude 16°N (Figure 6a–h). The reason for the positive bias may be connected to the method and type of parameterization used in COSMO (Baldauf et al., 2011). The daily variability is also not consistent between ERAI and the model. For example, the model reduces the buoyancy (CAPE) over areas south of 12°N in Nigeria, major areas in Burkina Faso, across Guinea, Liberia Sierra-Leone, and the Ivory Coast (Figure 2d,f,h,j,l,n,p). On the other hand, daily variability in CAPE tendency from 24 to 26 August is well captured by the COSMO over many areas across West Africa (Figure 2d,f,h,j,l,n,p). Despite the inherent deviations between COMSO simulations and ERAI, the model simulations (Figure 8a) have a

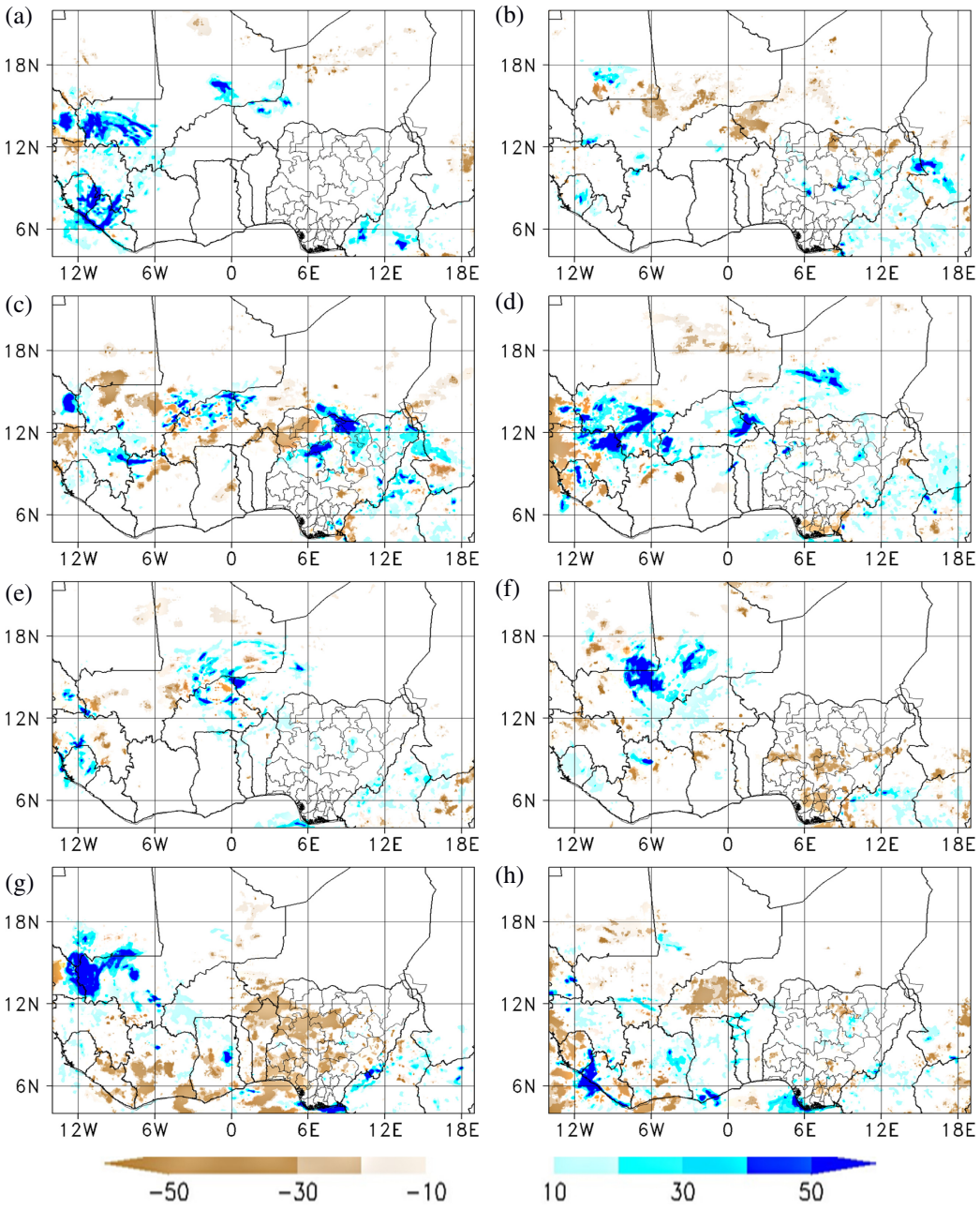

FIGURE 12 Daily rainfall bias between COSMO and GPM-IMERG from (a) 19 to (h) 26th August 2017. COSMO, Consortium for Small-scale Modelling; GPM-IMERG, Integrated Multi-satellite Retrieval for Global Precipitation Measurement.

correlation skill of above 0.5 in many places across West Africa, but a higher correlation skill over Nigeria, Togo, Ghana, and Ivory Coast. With a correlation skill of above 0.8 (Figure 7b), the model can reproduce the variability of the MSLP. This is despite a bias range of −1 to +1 hPa in areas south of 16°N (Figure 8). The daily evolution, the westward propagation, and the strength of both the AEJ and AEW trough are adequately captured by COSMO as depicted in Figures 9 and 10. However, the model also displays distinct differences at various levels. Despite being generally stronger, the model also spatially displaced the AEJ core about 200–600 km behind the observed AEJ, as shown in Figure 9, and occasionally about 200 km above the observed AEJ (Figure 9f). Similarly, the average location of the AEW trough as simulated by the COSMO usually lags behind the observed AEW trough, as shown in Figure 10 and Table 1.

3.3 | Daily rainfall

The daily spatial rainfall distribution in the COSMO simulations and the GPM is shown in Figure 11. COSMO

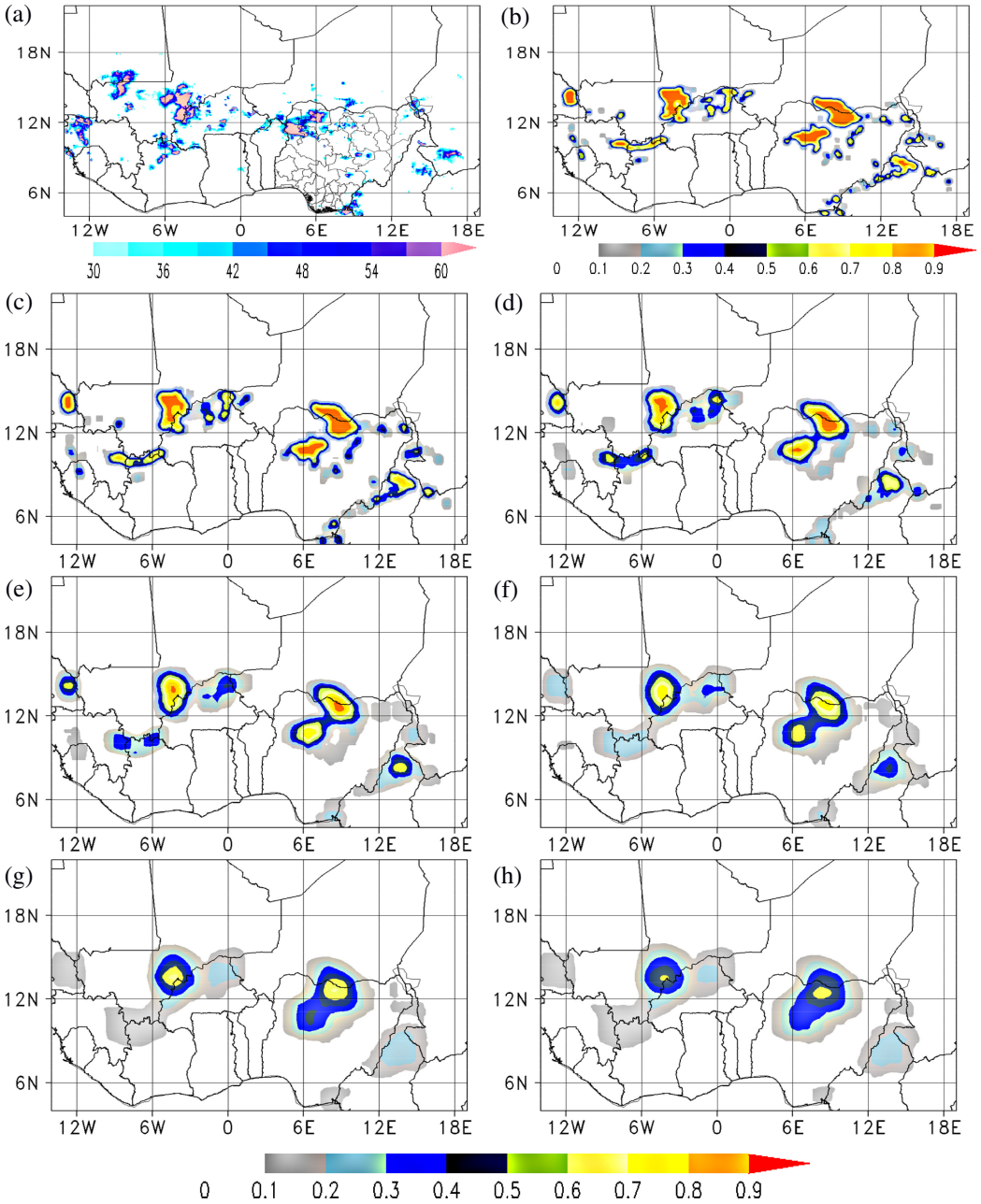

FIGURE 13 (a) Observed rainfall accumulation based on GPM-IMERG and the forecast fraction probability on 21 August for rainfall threshold of 30 mm based on neighbourhood size of (b) 50, (c) 70, (d) 110, (e) 150 km, (f) 210, (g) 270, (h) 310 km, respectively. GPM-IMERG, Integrated Multi-satellite Retrieval for Global Precipitation Measurement.

can capture the daily spatial rainfall distribution with contrasts in patterns over different regions for each day.

COSMO has also shown considerable biases. For instance, as shown in Figure 12, areas where the model overestimates and underestimates the observed rainfall greater than 30 mm are mostly areas where COSMO displays spatial deviations.

Forecast fractions calculated from GPM and COSMO are shown in Figure 13 for the daily rainfall accumulation exceeding 30 mm on 21 August 2017. Just from a visual comparison, it seems that by increasing the spatial scale from 30 to 310 km, the resemblance of the observed and predicted rainfall pattern increases. In other words, the spatial displacement between the two fields decreases with the spatial scale. FSS values, shown in Figure 14, confirm what a human forecaster would gauge by eye. FSS has been calculated for different increasing spatial scales of 30, 50, 70, 110, 150, 210, 270, and 310 km and different sub-regions and days for the probabilistic forecasts of rainfall accumulation exceeding the 95th percentile. FSS for Nigeria on 21 August 2017 shows

that the useful scale is reached at around 270 km, whereas FSS values over northern Nigeria for 25 August increase with neighbourhood size but remain below the 0.5 thresholds up to 310 km. The cases of Sierra Leone-Liberia on 26 August and of Senegal-Guinea-Sierra Leone on 22 August 2017 are the most skillful, with FSS values greater than 0.5 at all spatial scales. In other words, the forecast skill is shown to be higher in the regions west of the prime meridian and higher east of the prime meridian.

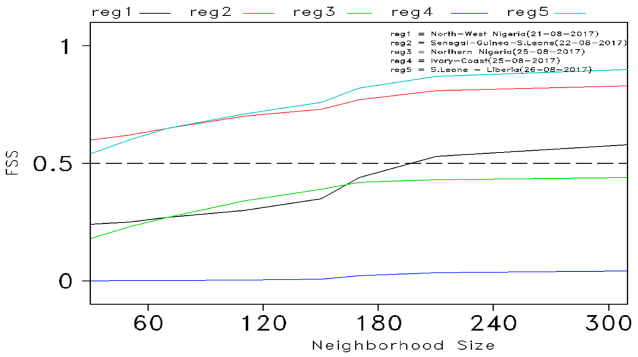

FIGURE 14 The fractions skill score based on the 95th percentile over the selected regions (see legend) of different neighbourhood sizes in km.

4 | HEAVY RAINFALL EVENT IN AUGUST 2015

Several flash floods occurred over West Africa between 17 and 22 of August 2015 as a result of the passage of a series of MCSs. In Nigeria, for example, floods affected 37,610 hectares of farmland, 5495 houses, and 25,950 people in 12 local government areas of Kebbi. Other affected Nigerian states include Bauchi, Adamawa, Anambra, Benue, Delta, Kaduna, Kebbi, Niger, Ondo,

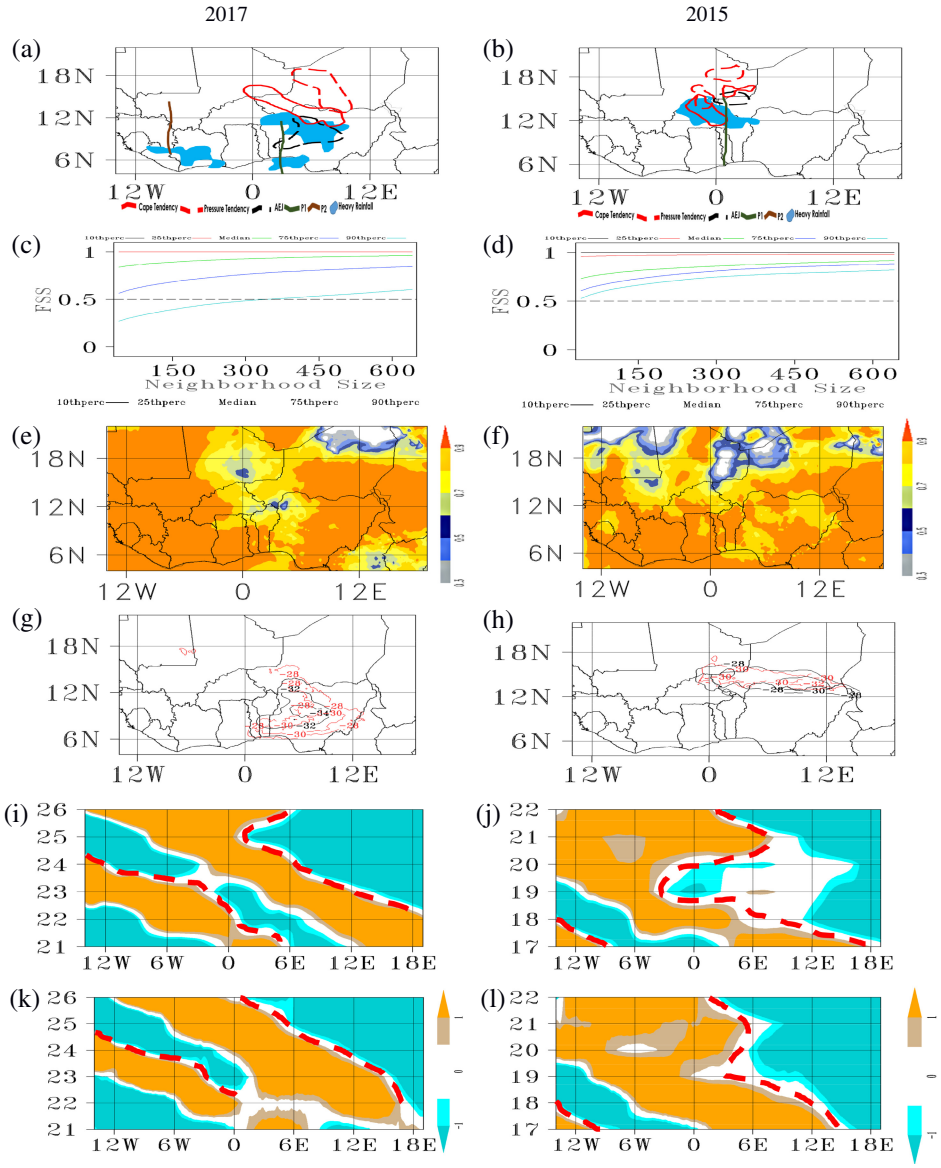

FIGURE 15 The synthetic analysis shows the main drivers of the heavy precipitation events occurring on (a) 25 August 2017 and (b) 17 August 2015. The legend is the same as in Figure 5. The COSMO FSS is based on the 10th (black line), 25th (red line), 50th (green line), 75th (blue line), and 90th (cyan line) percentile over West Africa on (c) 25 August 2017 and (d) 17 August 2015. The correlation between COSMO and MSLP is shown in (e) for 21–26 August 2017 and (f) for 17–22 August 2017. The spatial position of the AEJ core at 600 hPa is shown in (g) on 25 August 2017 and in (h) on 17 August 2015. The longitude-time (days in August 2015 and 2017) plots displaying the AEW through as dashed red lines are shown in (i,j) based on ERAI and (k, l) COSMO data for 21–26 August 2017 and 17–22 August 2015. AEJ, Africa Easterly Jet; AEW, Africa Easterly Wave; FSS, Fractions Skill Score; COSMO, Consortium for Small-scale Modelling; MSLP, mean sea level pressure.

Sokoto, Taraba, and Zamfara, with approximately 50 reported deaths and over 100,000 displaced (https://reliefweb.int/disaster/fl-2015-000155-nga). Burkina Faso is another affected area in West Africa with distinct loss of property (https://reliefweb.int/disaster/fl-2015-000106-bfa).

To put the paper's key findings to the test, we compare the results of the HIW event in August 2015 to those of the HIW event in August 2017, which is the focus of the paper. The synthetic analysis (Figure 15a,b) shows that the spatio-temporal characteristics of rainfall and the modulating drivers for both events are consistent. COSMO is able to predict the modulating drivers in both years in a consistent way. For example, as shown in Figure 15c,d, the model FSS improves significantly with increasing neighbourhood size over West Africa. The model also demonstrates strong correlation skill in predicting MSLP over West Africa irrespective of the year (Figure 15e,f). Additionally, as shown in Figure 15g–l, COSMO is consistent in both years in predicting the longitudinal propagation and intensity of the AEJ and the AEW through. The comparison with only one additional case is not sufficient to generalize the results, but this comparison supports the idea that the results are not just valid for the case in August 2017. Analysing many heavy rainfall events will be the focus of a follow-on study.

5 | CONCLUSIONS

This study investigates the large-scale drivers of the heavy precipitation events over West Africa between 19 and 27 August 2017. The study analysed the dynamical drivers used in operational practice and their individual and collective teleconnection in modulating areas of heavy rainfall across West Africa. The study assesses the performance of COSMO in predicting areas of heavy rainfall and the associated atmospheric dynamics to reduce the model's inherent biases as a deterministic model. The study suggests that all modulating rainfall dynamics, the AEJ, as well as CAPE and MSLP tendencies, move in concert but ahead of the AEW trough. The position of these drivers is sequential. They are in order of lowest decreasing pressure, highest increasing CAPE, and AEJ core (Figure 5). In a northeast to southwest orientation, the position of the drivers could sometimes be such that areas with the least falling pressure are immediately ahead of the AEW trough, followed by areas of the most rising CAPE, and finally the AEJ core. This suggests that every driver has a unique modulating effect. While areas of heavy rainfall are not often associated with falling pressure, for example, they are frequently associated with areas of increasing CAPE. Similarly, consistent with previous studies (e.g., Payne & McGarry, 1977; Rowell & Milford, 1993), regions of heavy rainfall are often found within the AEJ pool ahead of the AEW trough that precedes it. The AEW trough appears to be a distinct dynamic feature associated with areas of heavy rainfall west of the prime meridian. While areas of heavy rainfall east of the prime meridian are mostly associated with the combined interaction of most atmospheric dynamics (AEJ, CAPE, MSLP, and AEW), the contribution of AEWs east of the prime meridian is not as salient for the location of heavy rainfall as to the west of the prime meridian, which is consistent with Bolton (1984).

The results of assessing the model's skill in simulating synoptic-scale drivers revealed that COSMO can capture the large-scale dynamics over West Africa. Although the reproducibility of the AEJ and AEW trough exhibits spatial deviation by lagging behind the observed positions, COSMO can predict their daily evolution and intensity. While the model correlation skill in predicting CAPE and CAPE tendency is good and consistent over Nigeria, COSMO is able to predict the spatio-temporal evolution of MSLP and the pressure tendency with correlation skill greater than 0.85 in most places.

In simulating daily rainfall variability, the study showed that the COSMO forecasts reduce in skill as rainfall value tends to 30 mm. Despite the displayed spatio-temporal biases, most areas still have a correlation skill greater than 0.5. The results of correcting these biases (spatial displacement and underestimation) revealed a considerable improvement in the FSS as the neighbourhood size increases. Generally, the ability of COSMO to predict MSLP tendency is advantageous to operational forecasters. Therefore, the use of the COSMO for operational forecasting to assess areas of heavy rainfall could have two implications as a result of this study. First, forecasters could determine likely areas with heavy rainfall by estimating the position of the AEJ core from the knowledge of the position of areas of the least falling pressure from the COSMO forecast. Second, the neighbourhood forecast fraction could provide an additional tool. Forecasters can utilize this method to produce probabilistic forecasts from a deterministic model with no additional costs, with the advantage of having the assessment of the spatial uncertainty related to the event. Also, the FSS metric has been shown to give credits to forecasts that spatially look closer to observations by the human eye; therefore, the FSS is a metric that should be easy to interpret by local forecasters. Furthermore, it could help them to decide at which scale the forecasts should be issued for severe weather alerts.

In this study, we recognize that it would be interesting to investigate different cases during the monsoon season, as well as other seasons. However, such a thorough examination is beyond the scope of this paper and will be

the subject of a subsequent paper. This paper focuses on the heavy precipitation event between 19 and 26 August 2017 and was chosen as a cross-cutting case study as part of the GCRF-African SWIFT project. We have found that the sequence and location of CAPE and MSLP tendency, the AEJ core, and the position of the AEW through can be used by forecasters who have only access to fairly coarse model simulation with parameterized convection to predict the occurrence of heavy rainfall events.

AUTHOR CONTRIBUTIONS

Eniola A. Olaniyan: Conceptualization (lead); data curation (lead); formal analysis (lead); investigation (lead); methodology (lead); software (lead); validation (lead); visualization (lead); writing – original draft (lead). **Carlo Cafaro:** Methodology (supporting); software (supporting). **Stephen B. Ogungbenro:** Conceptualization (supporting); methodology (supporting). **Imoleayo E. Gbode:** Conceptualization (supporting); methodology (supporting). **Vincent O. Ajayi:** Conceptualization (supporting); methodology (supporting). **Ayodeji Oluleye:** Conceptualization (supporting); methodology (supporting). **Elijah A. Adefisan:** Conceptualization (supporting); methodology (supporting). **Juliane Schwendike:** Methodology (supporting); supervision (lead); visualization (supporting); writing – review and editing (supporting). **kamoru A. Lawal:** Conceptualization (supporting); data curation (supporting); methodology (supporting); writing – review and editing (supporting).

ACKNOWLEDGEMENT

This work was supported by the U.K. Research and Innovation as part of the Global Challenges Research Fund, Grant NE/P021077/1 (GCRF African SWIFT). We would like to thank Thorwald Stein for his comments and suggestions on the paper.

ORCID

Eniola A. Olaniyan https://orcid.org/0000-0003-0743-9860

REFERENCES

Afiesimama, E.A. (2007) Annual cycle of the mid-tropospheric easterly jet over West Africa. *Theoretical and Applied Climatology.*, 90, 103–111. https://doi.org/10.1007/s00704-006-0284-y

Akkermans, T., Böhme, T., Demuzere, M., Crewell, S., Selbach, C., Reinhardt, T. et al. (2012) Regime-dependent evaluation of accumulated precipitation in COSMO. *Theoretical and Applied Climatology*, 108(1–2), 39–52. https://doi.org/10.1007/s00704-011-0502-0

Baldauf, M., Seifert, A., Förstner, J., Majewski, D., Raschendorfer, M. & Reinhardt, T. (2011) Operational convective-scale numerical weather prediction with the COSMO model: description and sensitivities. *Monthly Weather Review*, 139(12), 3887–3905. https://doi.org/10.1175/MWR-D-10-05013.1

Bolton, D. (1984) Generation and propagation of African squall lines. *Quarterly Journal of the Royal Meteorological Society*, 110, 695–721.

Bongioannini Cerlini, P., Emanuel, K.A. & Todini, E. (2005) Orographic effects on convective precipitation and space-time rainfall variability: preliminary results. *Hydrology and Earth System Sciences*, 9(4), 285–299. https://doi.org/10.5194/hess-9-285-2005

Cafaro, C., Woodhams, B.J., Stein, T.H.M., Birch, C.E., Webster, S., Bain, C.L. et al. (2021) Do convection-permitting ensembles lead to more skillful short-range probabilistic rainfall forecasts over tropical East Africa? *Weather and Forecasting*, 36(2), 697–716. https://doi.org/10.1175/WAF-D-20-0172.1

Chen, J., Dai, A., Zhang, Y. & Rasmussen, K.L. (2020) Changes in convective available potential energy and convective inhibition under global warming. *Journal of Climate*, 33(6), 2025–2050. https://doi.org/10.1175/JCLI-D-19-0461.1

Clark, A.J., Gallus, W.A., Xue, M. & Kong, F. (2009) A comparison of precipitation forecast skill between small convection-allowing and large convection-parameterizing ensembles. *Weather and Forecasting*, 24(4), 1121–1140. https://doi.org/10.1175/2009WAF2222222.1

Cook, K.H. (1999) Generation of the African easterly jet and its role in determining West African precipitation. *Journal of Climate*, 12, 1165–1184. https://doi.org/10.1175/1520-0442(1999)012<1165:GOTAEJ>2.0.CO;2

Cuo, L., Pagano, T.C. & Wang, Q.J. (2011) A review of quantitative precipitation forecasts and their use in short- to medium-range streamflow forecasting. *Journal of Hydrometeorology*, 12(5), 713–728. https://doi.org/10.1175/2011JHM1347.1

Diedhiou, A., Janicot, S., Viltard, A., De Felice, P. & Laurent, H. (1999) Easterly wave regimes and associated convection over West Africa and tropical Atlantic: results from the NCEP/NCAR and ECMWF reanalyses. *Climate Dynamics*, 15(11), 795–822. https://doi.org/10.1007/s003820050316

Fischer, M.S., Rogers, R.F. & Reasor, P.D. (2020) The rapid intensification and eyewall replacement cycles of Hurricane Irma (2017). *Monthly Weather Review*, 148(3), 981–1004. https://doi.org/10.1175/MWR-D-19-0185.1

Gartzke, J., Knuteson, R., Przybyl, G., Ackerman, S. & Revercomb, H. (2017) Comparison of satellite-, model-, and radiosonde-derived convective available potential energy in the Southern Great Plains region. *Journal of Applied Meteorology and Climatology*, 56(5), 1499–1513. https://doi.org/10.1175/JAMC-D-16-0267.1

Giannini, A., Saravanan, R. & Chang, P. (2003) Oceanic forcing of Sahel rainfall on interannual to interdecadal time scales. *Science*, 302(5647), 1027–1030.

Gilleland, E., Ahijevych, D., Brown, B.G., Casati, B. & Ebert, E.E. (2009) Intercomparison of spatial forecast verification methods. *Weather and Forecasting*, 24(5), 1416–1430. https://doi.org/10.1175/2009WAF2222269.1

Groenemeijer, P. & Craig, G.C. (2012) Ensemble forecasting with a stochastic convective parametrization based on equilibrium statistics. *Atmospheric Chemistry and Physics*, 12(10), 4555–4565. https://doi.org/10.5194/acp-12-4555-2012

Grogan, D.F.P., Nathan, T.R. & Chen, S.H. (2017) Saharan dust and the nonlinear evolution of the African easterly jet-African easterly wave system. *Journal of the Atmospheric Sciences*, 74(1), 27–47. https://doi.org/10.1175/JAS-D-16-0118.1

Hanley, K.E., Pirret, J.S., Bain, C.L., Hartley, A.J., Lean, H.W., Webster, S. et al. (2021) Assessment of convection-permitting versions of the

unified model over the Lake Victoria basin region. *Quarterly Journal of the Royal Meteorological Society*, 147(736), 1642–1660.

Hauck, C., Barthlott, C., Krauss, L. & Kalthoff, N. (2011) Soil moisture variability and its influence on convective precipitation over complex terrain. *Quarterly Journal of the Royal Meteorological Society*, 137(SUPPL. 1), 42–56. https://doi.org/10.1002/qj.766

Hoerling, M., Hurrel, J., Eischeid, J. & Phillips, A. (2006) Detection and attribution of twentieth-century northern and southern African. *American Meteorological Society*, 19(16), 3989–4008.

Kain, J. & Michael, F. (1990) A one-dimensional entraining/detraining plume model and its application in convective parameterization. *Journal of the Atmospheric Sciences*, 47(23), 2784–2802.

Kimberlain, T.B., Blake, E.S. & Cangialosi, P. (2015) *National Hurricane Center tropical cyclone report. Hurricane Patricia*. *National Hurricane Center*, pp. 1–32.

Kober, K., Foerster, A.M. & Craig, G.C. (2015) Examination of a stochastic and deterministic convection parameterization in the COSMO model. *Monthly Weather Review*, 143(10), 4088–4103. https://doi.org/10.1175/MWR-D-15-0012.1

Kowaleski, A.M., Morss, R.E., Ahijevych, D. & Fossell, K.R. (2020) Using a WRF-ADCIRC ensemble and track clustering to investigate storm surge hazards and inundation scenarios associated with Hurricane Irma. *Weather and Forecasting*, 35(4), 1289–1315. https://doi.org/10.1175/WAF-D-19-0169.1

Lavaysse, C., Flamant, C., Janicot, S., Parker, D.J., Lafore, J.P., Sultan, B. et al. (2009) Seasonal evolution of the West African heat low: a climatological perspective. *Climate Dynamics.*, 33, 313–330. https://doi.org/10.1007/s00382-009-0553-4

Lin, Y.L., Farley, R.D. & Orville, H.D. (1983) Bulk parameterization of the snow field in a cloud model. *Journal of Applied Meteorology and Climatology*, 22(6), 1065–1092.

Majewski, D., Liermann, D., Prohl, P., Ritter, B., Buchhold, M., Hanisch, T. et al. (2002) The operational global icosahedral-hexagonal gridpoint model GME: description and high-resolution tests. *Monthly Weather Review*, 130(2), 319–338. https://doi.org/10.1175/1520-0493(2002)130<0319:TOGIHG>2.0.CO;2

Maranan, M., Fink, A.H., Knippertz, P., Amekudzi, L.K., Atiah, W.A. & Stengel, M. (2020) A process-based validation of GPM IMERG and its sources using a mesoscale rain gauge network in the West African forest zone. *Journal of Hydrometeorology*, 21(4), 729–749. https://doi.org/10.1175/JHM-D-19-0257.1

Maurer, V., Kalthoff, N. & Gantner, L. (2017) Predictability of convective precipitation for West Africa: verification of convection-permitting and global ensemble simulations. *Meteorologische Zeitschrift*, 26(1), 93–100. https://doi.org/10.1127/metz/2016/0728

Mellor, G.L. & Yamada, T. (1982) Development of a turbulence closure model for geophysical fluid problems. *Reviews of Geophysics*, 20(4), 851–875.

Mironov, D. & Raschendorfer, M. (2001) *Evaluation of empirical parameters of the new LM surface-layer parameterization scheme: results from numerical experiments including the soil moisture analysis*. DWD. https://doi.org/10.5676/DWD_pub/nwv/cosmo-tr_1

Olaniyan, E. & Afiesimama, E. (2015) Simulating the daily evolution of west African monsoon using high resolution regional Cosmo-model: a case study of the first half of 2015 over Nigeria. *Journal of Climatology & Weather Forecasting*, 03, 1-8. https://doi.org/10.4172/2332-2594.1000142

Olaniyan E., Adefisan E.A., Balogun A.A. & Lawal K.A. (2019) The influence of global climatedrivers on monsoon onset variability in Nigeria using S2S models. *Modeling Earth Systems and Environment*, 5, 1405–1428. https://doi.org/10.1007/s40808-019-00606-x

Parker, D.J., Blyth, A.M., Woolnough, S.J., Dougill, A.J., Bain, C.L., de Coning, E. et al. (2021) The African SWIFT project: growing science capability to bring about a revolution in weather prediction. *Bulletin of the American Meteorological Society*, 103(2), 1–53. https://doi.org/10.1175/bams-d-20-0047.1

Payne, S.W. & McGarry, M.M. (1977) The relationship of satellite inferred convective activity to easterly waves over West Africa and the adjacent ocean during phase III of GATE. *Monthly Weather Review*, 105(4), 413–420.

Rakesh, V. & Goswami, P. (2016) An evaluation strategy of skill of high-resolution rainfall forecast for specific agricultural applications. *Meteorological Applications*, 23(3), 529–540. https://doi.org/10.1002/met.1576

Ritter, B. & Geleyn, J.F. (1992) A comprehensive radiation scheme for numerical weather prediction models with potential applications in climate simulations. *Monthly Weather Review*, 120(2), 303–325.

Roberts, N.M. & Lean, H.W. (2008) Scale-selective verification of rainfall accumulations from high-resolution forecasts of convective events. *Monthly Weather Review*, 136(1), 78–97. https://doi.org/10.1175/2007MWR2123.1

Rowell, D.P. & Milford, J.R. (1993) On the generation of African squall lines. *Journal of Climate*, 6(6), 1181–1193.

Saito, K., Fujita, T., Yamada, Y., Ishida, J.I., Kumagai, Y., Aranami, K. et al. (2006) The operational JMA nonhydrostatic mesoscale model. *Monthly Weather Review*, 134(4), 1266–1298. https://doi.org/10.1175/MWR3120.1

Senkbeil, J., Collins, J. & Reed, J. (2019) Evacuee perception of geophysical hazards for hurricane Irma. *Weather, Climate, and Society*, 11(1), 217–227. https://doi.org/10.1175/WCAS-D-18-0019.1

Sivakumar, M.V.K. (2006) Dissemination and communication of agrometeorological information—global perspectives. *Meteorological Applications*, 13(S1), 21–30. https://doi.org/10.1017/S1350482706002520

Skofronick-Jackson, G., Petersen, W.A., Berg, W., Kidd, C., Stocker, E.F., Kirschbaum, D.B. et al. (2017) The global precipitation measurement (GPM) mission for science and society. *Bulletin of the American Meteorological Society*, 98(8), 1679–1695. https://doi.org/10.1175/BAMS-D-15-00306.1

Skok, G. & Roberts, N. (2016) Analysis of fractions skill score properties for random precipitation fields and ECMWF forecasts. *Quarterly Journal of the Royal Meteorological Society*, 142(700), 2599–2610.

Staniforth, A. & Wood, N. (2008) Aspects of the dynamical core of a nonhydrostatic, deep-atmosphere, unified weather and climate-prediction model. *Journal of Computational Physics*, 227(7), 3445–3464.

Stein, T.H.M., Keat, W., Maidment, R.I., Landman, S., Becker, E., Boyd, D.F.A. et al. (2019) An evaluation of clouds and precipitation in convection-permitting forecasts for South Africa. *Weather and Forecasting*, 34(1), 233–254. https://doi.org/10.1175/WAF-D-18-0080.1

Theis, S.E., Hense, A. & Damrath, U. (2005) Probabilistic precipitation forecasts from a deterministic model: a pragmatic approach. *Meteorological Applications*, 12(3), 257–268. https://doi.org/10.1017/S1350482705001763

Tiedtke, M. (1989) A comprehensive mass flux scheme for cumulus parameterization in large-scale models. *Monthly Weather Review*, 117(8), 1779–1800.

Wacker, U., Ries, H. & Schättler, U. (2009) Precipitation simulation for dronning maud land using the COSMO model. *Antarctic Science*, 21(6), 643–662. https://doi.org/10.1017/S0954102009990149

Washington, R., Harrison, M., Conway, D., Black, E., Challinor, A., Grimes, D. et al. (2006) African climate change: taking the shorter route. *Bulletin of the American Meteorological Society*, 87(10), 1355–1366.

Woodhams, B.J., Birch, C.E., Marsham, J.H., Bain, C.L., Roberts, N. M. & Boyd, D.F.A. (2018) What is the added value of a convection-permitting model for forecasting extreme rainfall over tropical East Africa? *Monthly Weather Review*, 146(9), 2757–2780. https://doi.org/10.1175/MWR-D-17-0396.1

Wu, T., Yu, R., Zhang, F., Wang, Z., Dong, M., Wang, L. et al. (2010) The Beijing climate center atmospheric general circulation model: description and its performance for the present-day climate. *Climate Dynamics*, 34(1), 123–147. https://doi.org/10.1007/s00382-008-0487-2

Zeng, N., Neelin, J.D., Lau, K.M. & Tucker, C.J. (1999) Enhancement of interdecadal climate variability in the Sahel by vegetation interaction. *Science*, 286(5444), 1537–1540.

Ziarani, M.R., Bookhagen, B., Schmidt, T., Wickert, J., de la Torre, A. & Hierro, R. (2019) Using convective available potential energy (CAPE) and dew-point temperature to characterize rainfall-extreme events in the SOUTHCENTRAL ANDES. *Atmosphere*, 10(7), 1–22. https://doi.org/10.3390/atmos10070379

How to cite this article: Olaniyan, E. A., Cafaro, C., Ogungbenro, S. B., Gbode, I. E., Ajayi, V. O., Oluleye, A., Adefisan, E. A., Schwendike, J., & Lawal, K. A. (2022). Performance evaluation of a high-resolution regional model over West Africa for operational use: A case study of August 2017. *Meteorological Applications*, *29*(4), e2080. https://doi.org/10.1002/met.2080